Pamukkale Univ Muh Bilim Derg, 31(8), 1439-1455, 2025
(Special Issue of the 10th Geochemistry Symposium)

Pamukkale Üniversitesi Mühendislik Bilimleri Dergisi

Pamukkale University Journal of Engineering Sciences

Mineralogical-Petrographic characteristics of garnet porphyroblasts (Ekinözü-Kahramanmaraş), determination of metamorphism conditions and gemstone potential

Granat porfiroblastlarının (Ekinözü-Kahramanmaraş) mineralojik-petrografik özellikleri, metamorfizma koşullarının belirlenmesi ve süs taşı potansiyeli

Ufuk Ören[1*], *Tamer Koralay*[2]

[1]Department of Handicrafts, Karacasu Memnune İnci Vocational School, Aydın Adnan Menderes University, Aydın, Türkiye.
ufukoren@adu.edu.tr

[2]Department of Geological Engineering, Faculty of Engineering, Pamukkale University, Denizli, Türkiye.
tkoralay@pau.edu.tr

Received/Geliş Tarihi: 05.09.2025 Revision/Düzeltme Tarihi: 03.11.2025 doi: 10.65206/pajes.02817
Accepted/Kabul Tarihi: 03.11.2025 Special Issue Article/Özel Sayı Makalesi

Abstract

The studied garnet porphyroblasts occur within metamorphic rocks consisting of schists with variable mineralogical compositions in the Ekinözü (Kahramanmaraş) region. The porphyroblasts crystallized in pentagonal dodecahedron forms, ranging in size from 0.5 to 4 cm and exhibit dark red to reddish-black colors with vitreous luster. Microscopic observations reveal that the garnet porphyroblasts display a highly fractured and cracked texture, containing inclusions of quartz, chlorite and opaque minerals such as ilmenite-magnetite. Confocal Raman spectroscopy analyses indicate that the garnet porphyroblasts are of almandine composition. Their chemical structural formulas were determined as $Alm_{0.80\text{-}0.88}Prp_{0.07\text{-}0.13}Grs_{0.01\text{-}0.07}Sps_{0.00\text{-}0.05}$*. Garnet-biotite geothermometry calculations suggest that the garnets crystallized under average pressure conditions of ~4.5 kbar at temperatures of 465.4±41.6 °C. Multi-element variation diagrams normalized to the lower and upper continental crust indicate depletion in LIL elements (Sr, K, Rb and Ba), whereas enrichment is observed in HFS elements (Ta, P, Zr, Hf and Y). Chondrite-normalized multi-element diagrams show up to 100-fold enrichment in Rare Earth Elements (REE) (∑REE: 162.1-284.9;* $(La/Sm)_N$ *= 1.65-3.62;* $(Sm/Yb)_N$ *= 0.43-0.67). Enrichment Factor (EF) calculations from chemical analyses highlight the role of Co, Fe, U and Mn elements in color development. These findings are further supported by EPMA data and optical absorption spectroscopy, both of which confirm the predominant presence of* Fe^{+2} *ions. Mineralogical, geochemical and gemological investigations indicate that the Ekinözü garnet porphyroblasts formed under greenschist facies metamorphic conditions. Their euhedral crystal morphology, together with their dark red coloration and vitreous luster, suggests that these garnets have potential for use as gemstones in jewelry.*

Keywords: Garnet porphyroblasts, Raman spectroscopy, Mineral chemistry, Gemology, Gemstone.

Öz

Çalışma konusu olan granat porfiroblastları Ekinözü (Kahramanmaraş) bölgesinde farklı mineralojik bileşime sahip şistlerden oluşan metamorfik kayaçlar içerisinde bulunmaktadır. Pentagonal dodekahedron formda kristallenmiş olan granat porfiroblastlarının boyutları 0.5 - 4 cm arasında değişmekte olup koyu kırmızı, kırmızımsı siyah renkte camsı parlaklığa sahiptirler. Mikroskop incelemelerinde oldukça kırıklı-çatlaklı bir yapıda olan granat porfiroblastları kuvars, klorit ve ilmenit-manyetit türü opak mineral kapanımları içermektedir. Konfokal Raman spektroskopisi analizlerine göre granat porfiroblastları almandin bileşimindedirler. Granat porfiroblastlarının kimyasal yapı formülleri $Alm_{0.80\text{-}0.88}Prp_{0.07\text{-}0.13}Grs_{0.01\text{-}0.07}Sps_{0.00\text{-}0.05}$ *olarak belirlenmiştir. Granat-biyotit jeotermometre sonuçları, granatların yaklaşık 4.5 kbar basınç ve 465.4±41.6 °C sıcaklık koşullarında kristalleştiklerini göstermektedir. Alt ve üst kıta kabuğu değerlerine göre normalleştirilmiş çoklu element diyagramları, Ekinözü granat porfiroblastlarının LIL elementleri (Sr, K, Rb ve Ba) açısından tüketildiğini, buna karşılık HFS elementleri (Ta, P, Zr, Hf ve Y) yönünden zenginleştiğini ortaya koymaktadır. Çoklu elementlerin kondrite normalize edilerek değerlendirildiği diyagramlarda, granat porfiroblastlarının Nadir Toprak Element bakımından yaklaşık 100 kata ulaşan zenginleşmeler gösterdiği saptanmıştır (∑NTE: 162.1-284.9; (*$(La/Sm)_N$*=1.65-3.62); (*$(Sm/Yb)_N$*=0,43-0,67). Kimyasal analizlerden elde edilen Zenginleşme Faktörü hesaplamaları, özellikle Co, Fe, U ve Mn elementlerinin renk oluşum sürecinde etkili olduğunu göstermektedir. EPMA analizleri ile optik absorpsiyon spektroskopisi de bu bulguları destekleyerek* Fe^{+2} *iyonunun baskın varlığını ortaya koymaktadır. Mineralojik, jeokimyasal ve gemolojik incelemeler sonucunda Ekinözü granat porfiroblastlarının yeşilşist fasiyesine karşılık gelen metamorfizma şartlarında oluştukları, öz şekilli kristal yapısına sahip olması ve koyu kırmızı renkte camsı parlaklık göstermesi nedeniyle mücevheratta kullanılabileceği değerlendirilmektedir.*

Anahtar kelimeler: Granat porfiroblastları, Raman spektroskopisi, Mineral kimyası, Gemoloji, Süs taşı.

1 Introduction

Garnets are minerals that hold a significant place in geological and mineralogical research worldwide and possess a wide range of applications. Initially used in jewelry and ornamental objects around 5000 years ago, garnets later gained industrial importance as their chemical and physical properties became better understood. Classified as a group of minerals, garnets are complex silicates characterized by a wide chemical compositional range and similarities in crystal structure. Their general chemical formula is expressed as $X_3Y_2(SiO_4)_3$ and they are subdivided into various groups depending on the elements

*Corresponding author/Yazışılan Yazar

occupying the X and Y positions. These minerals commonly form isomorphic series containing elements such as aluminum, iron, magnesium, calcium, manganese, and chromium. Almandine, pyrope, grossular, spessartine, andradite, and uvarovite are among the most well-known garnet varieties. Belonging to the isometric crystal system, garnets typically develop as dodecahedral or trapezohedral crystals and exhibit highly isotropic optical properties. Their formation largely depends on metamorphic and, to a lesser extent, magmatic environments. Garnets that grow as porphyroblasts in rocks such as schists, gneisses, and amphibolites under regional metamorphism are important petrogenetic indicators of temperature and pressure conditions within the mineral assemblage. Medium- to high-grade metamorphic facies, in particular, provide favorable conditions for garnet growth and the development of core-to-rim zoning. Since their chemical composition reflects these conditions, garnets are frequently utilized in geothermobarometric calculations. Garnets also occur in granitic pegmatites and some ultramafic rocks, where they typically form larger crystals with distinct geochemical characteristics. In addition, metasomatic processes, hydrothermal activity, and partial melting contribute to garnet formation, while rare types are also found in carbonatites and skarn zones. Garnet minerals are of importance not only geologically but also economically and technologically. Their relatively high hardness (Mohs 6.5-7.5) makes them widely used as abrasives in water-jet cutting systems and in the production of sandpaper. Furthermore, their transparent and colored varieties have long been valued as gemstones, utilized for aesthetic and symbolic purposes across various cultures from antiquity to the present day. In optics, garnet-based glasses are used to produce specialized lenses and filters due to their distinct densities and refractive indices [1]-[12].

This study was designed to achieve two primary objectives. First, it aims to provide a detailed characterization of the mineralogical, petrographic, and geochemical features of garnet porphyroblasts developed within medium to high-grade metamorphic rocks in the Ekinözü region of Kahramanmaraş Province. The second objective is to evaluate whether the euhedral garnet porphyroblasts observed in the study area can be utilized as gemstones and to present a scientific assessment of this potential. It should be emphasized that studies investigating such garnet occurrences through multi-analytical approaches remain quite limited in Türkiye. In this context, interdisciplinary research integrating complementary analytical techniques such as optical microscopy, X-ray diffraction (XRD), confocal Raman spectroscopy (CRS), electron probe microanalysis (EPMA), and inductively coupled plasma mass spectrometry (ICP-MS) is of critical importance for filling the knowledge gap in this field.

2 Geological setting

The study area is located around Türkmenler Village, approximately 12 km southwest of the Ekinözü district in Kahramanmaraş Province. It lies within the boundaries of the 1:100,000 scale Gaziantep-M38 topographic map. The region is predominantly composed of metamorphic and sedimentary rock assemblages. Garnet crystals are observed as porphyroblastic structures within the metamorphic units of this area.

The stratigraphic succession of the study area and its surroundings, in chronological order, can be summarized as follows: Lower Paleozoic gneisses, mica schists and migmatites; followed by Devonian dolomitic limestones and marbles; Permian cherty limestones together with Upper Permian dolomitic marbles and recrystallized limestones; Upper Permian-Middle Triassic marble-calc-schist levels; and finally, Upper Cretaceous units consisting of serpentinites, peridotites and a sedimentary sequence of sandstones, siltstones, claystones and shales, completing the stratigraphic succession (Figure 1) [13],[14].

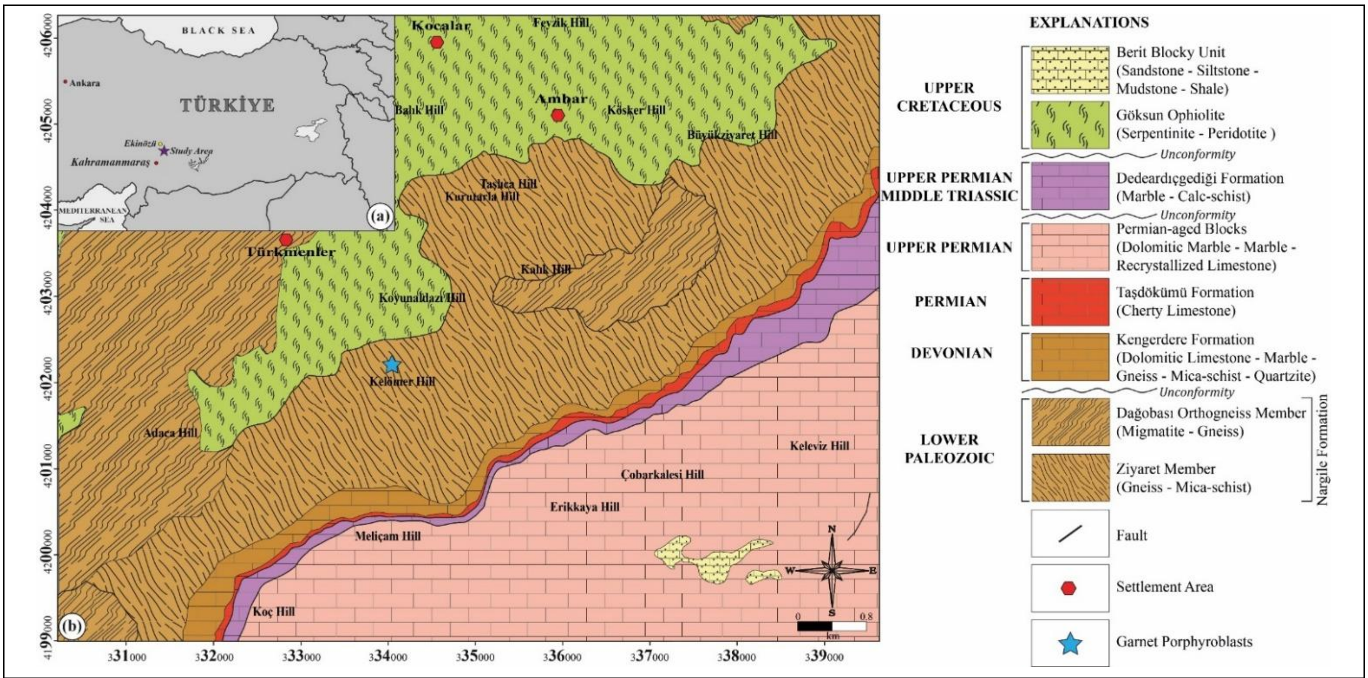

Figure 1. Geological map of the research area (adapted from MTA, 1:100000 scale, Gaziantep-M38 map).

The oldest lithological units exposed in the study area belong to the Lower Paleozoic Nargile Formation, represented by the Ziyaret Member and the Dağobası Orthogneiss Member. The Ziyaret Member, which hosts garnet porphyroblasts, consists mainly of gneisses and mica schists. The Dağobası Member, on the other hand, comprises migmatites and gneisses with cataclastic textures and mineral assemblages including quartz, albite, oligoclase, pyroxene, and chlorite. In the northern part of the area, the Upper Cretaceous Göksun Ophiolite is exposed, consisting mainly of serpentinites and peridotites. In the western part of the area, the following lithological units are observed in succession: the Devonian Kengerdere Formation, represented by black to gray-colored, medium- to thick-bedded dolomitic limestones, marbles, gneisses, mica schists and quartzites; the Upper Permian-Middle Triassic Dedeardıçgediği Formation, comprising marbles and dolomitic limestones with yellow, purple and black color tones, medium- to thick-bedded layers, locally containing lamellibranch shells and bioturbation traces (worm burrows), as well as schists and quartzites; and Upper Permian blocks represented by dark gray, bluish-gray to locally white-colored, medium- to thick-bedded dolomitic marbles, semi-marbles and recrystallized limestones (Figure 1) [15]-[23].

3 Materials and methods

3.1 Sample description and gemological tests

Standard gemological tests were performed on garnet porphyroblasts obtained from the Ekinözü locality in Kahramanmaraş. These tests were carried out in the Gemology Laboratory of Aydın Adnan Menderes University, Karacasu Memnune İnci Vocational School (AMGL). Refractive index measurements were conducted using an Eickhorst M3 refractometer equipped with a 589 nm quartz lamp, while optical absorption spectra were recorded with an Eickhorst SPO-CF spectroscope operating in the 700-400 nm range. In addition, UV reactions and fluorescence-phosphorescence properties were examined using an Eickhorst UV 240 device (short-wave: 255 nm; long-wave: 366 nm; 4W UV lamp). The color properties of the garnets were determined using an NR60CP portable colorimeter, and the resulting visual data were converted to numerical color values. Within the schists, garnet crystals appear as porphyroblasts ranging from 0.5 to 4 cm in diameter, typically exhibiting pentagonal dodecahedral crystal morphology (Figure 2).

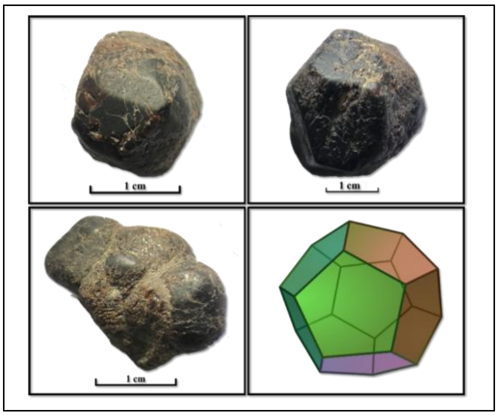

Figure 2. Hand specimens and the pentagonal dodecahedron crystal form of the Ekinözü garnet porphyroblasts.

These porphyroblasts display deep red to nearly black hues with vitreous luster and can be readily separated from the host rock through physical means.

3.2 Microscopic and spectroscopic investigations

Thin sections prepared for petrographic evaluation were analyzed at the Department of Geological Engineering, Pamukkale University, using a Carl Zeiss Primotech polarizing microscope capable of operating under both transmitted and reflected light.

To determine the structural and chemical components of garnets with higher precision and non-destructively, Confocal Raman Spectroscopy (CRS) was used. For this purpose, three polished garnet sections were examined using a DXR-2 confocal Raman spectrometer (Thermo Scientific), equipped with a 785 nm air-cooled argon laser. These analyses were carried out at the Earth Sciences Application and Research Center (YEBİM), Ankara University.

3.3 SEM analyses

Scanning Electron Microscopy (SEM) is a powerful imaging and analytical technique widely employed in mineralogical and gemological studies. Its major advantages include the ability to analyze samples non-destructively, minimal preparation requirements, high-resolution observation of surface morphology, and detailed characterization of surface inclusions and microstructural variations. In particular, the suitability of flat surfaces on faceted gemstones for analysis, together with SEM's ability to reveal internal structural features not detectable by conventional gemological methods, underscores the importance of this technique in gemological research. Moreover, the characterization of surface inclusions is critical for distinguishing natural from synthetic stones, making SEM imaging an effective tool for this purpose [24].

In this study, SEM analyses were employed to investigate the surface morphology and microtextural features of the garnets. Two garnet crystals selected from the locality were coated with carbon using a Quorum Q150T ES device and subsequently examined with a Tescan Tima/Mira SEM instrument. The SEM analyses were conducted at an accelerating voltage of 30 kV and a beam current of 30 nA, utilizing a secondary electron (SE) detector. Parameters such as magnification, beam diameter, working distance (WD), and field of view (FoV) were optimized to enhance image quality. The analyses were performed at the YEBİM, Ankara University.

3.4 XRD analyses

Beyond microscopic observations, X-ray powder diffraction (XRD) was conducted to identify mineral phases not visible to the naked eye and to reveal detailed variations in crystal structure. For this purpose, three garnet porphyroblasts and one host-rock sample were powdered using a tungsten carbide mill, and the analyses were performed at the Advanced Technology Application and Research Center (PAÜ-ILTAM), Pamukkale University, using a GNR APD 2000 XRD instrument. The device operated with Cu Kα radiation (λ = 1.54 Å) as the source. Measurements were carried out at 10-60 kV voltage, 5-60 mA current, with a scanning speed of 0.1° (2θ/s) and within a scanning range of -111° < 2θ < 168°.

3.5 Chemical analyses

To determine the bulk chemical compositions, Inductively Coupled Plasma-Mass Spectrometry (ICP-MS) analyses were performed. The samples were ground to 150-200 mesh using a tungsten carbide ring mill, and the grinding system was cleaned with an alcohol-water mixture between samples to prevent contamination. Powdered samples (0.5 g each) were digested in a 2:2:2 mixture of HNO_3-HCl-H_2O at 95 °C, and the analyses were conducted at ACME Analytical Laboratories (Canada). The results for garnet porphyroblasts and their host rock are presented in Table 1.

Table 1. Major oxide (wt%), trace element (ppm), and Rare Earth Element (REE)(ppm) analysis results of garnet porphyroblasts from the Ekinözü region and their host rock.

Element/Sample		Garnet Porphyroblasts					Host Rock
		KMGR-1	KMGR-2	KMGR-3	KMGR-4	KMGR-5	KMGR-YK
SiO_2	wt %	34.17	34.41	34.53	35.19	34.93	35.53
Al_2O3	wt %	20.29	20.23	20.10	20.34	20.35	15.77
Fe_2O_3	wt %	41.67	42.09	42.26	41.79	41.74	33.56
MgO	wt %	2.40	2.66	2.87	2.63	2.69	5.76
CaO	wt %	1.33	1.12	0.95	1.31	1.29	0.43
Na_2O	wt %	0.02	0.02	0.02	0.02	0.02	0.05
MnO	wt %	0.41	0.32	0.20	0.33	0.29	0.15
TiO_2	wt %	0.22	0.23	0.26	0.23	0.22	1.52
K_2O	wt %	0.06	0.05	0.01	0.04	0.02	1.29
P_2O_5	wt %	0.20	0.28	0.35	0.18	0.22	0.21
LOI	wt %	-1.1	-1.8	-1.8	-2.4	-2.2	5.2
Total	wt %	99.68	99.68	99.73	99.65	99.64	99.52
Cr	ppm	54.7	47.9	68.4	41.1	47.9	287.0
Ba	ppm	18.0	11.0	6.0	8.0	6.0	28.0
Ni	ppm	94.0	89.0	83.0	101.0	101.0	61.0
Sc	ppm	37.0	32.0	33.0	33.0	35.0	34.0
Co	ppm	187.3	192.5	140.2	211.0	208.8	95.1
Cs	ppm	<0.1	<0.1	<0.1	<0.1	<0.1	0.9
Ga	ppm	4.3	4.4	4.9	4.4	4.5	10.9
Hf	ppm	6.1	5.9	5.2	9.0	6.7	2.8
Nb	ppm	3.6	4.4	4.1	4.2	3.4	8.4
Rb	ppm	1.2	1.1	0.5	1.1	0.9	17.1
Sn	ppm	2.0	2.0	1.0	2.0	2.0	3.0
Sr	ppm	3.9	4.3	3.5	2.3	2.8	8.7
Ta	ppm	4.0	4.6	4.1	5.6	5.0	1.4
Th	ppm	11.3	12.2	9.5	13.6	12.5	6.2
U	ppm	3.8	3.8	3.0	5.0	5.4	10.0
V	ppm	25.0	25.0	30.0	23.0	26.0	175.0
Zr	ppm	225.4	223.6	196.6	326.1	255.3	105.2
Y	ppm	183.9	128.7	151.8	176.7	146.6	97.4
Mo	ppm	1.0	0.9	0.7	0.8	0.8	2.7
Cu	ppm	164.4	159.3	142.3	95.4	176.0	1280.7
Pb	ppm	0.5	0.4	0.5	0.3	0.3	1.0
Zn	ppm	5.0	2.0	2.0	3.0	3.0	18.0
As	ppm	<0.5	<0.5	<0.5	<0.5	<0.5	<0.5
Cd	ppm	<0.1	<0.1	<0.1	<0.1	<0.1	<0.1
La	ppm	26.7	26.8	16.8	15.1	50.2	209.8
Ce	ppm	54.9	57.0	37.5	29.8	91.7	375.4
Pr	ppm	6.5	6.8	4.9	4.0	11.1	40.2
Nd	ppm	24.9	25.5	19.0	16.6	40.4	132.8
Sm	ppm	7.1	6.9	5.4	5.7	8.7	23.4
Eu	ppm	3.6	2.9	1.7	3.0	3.5	7.6
Gd	ppm	16.7	12.8	11.6	15.3	14.5	21.3
Tb	ppm	3.9	2.8	3.0	3.6	3.2	3.0
Dy	ppm	28.5	19.7	23.1	26.8	23.2	17.4
Ho	ppm	6.3	4.3	5.3	5.8	5.0	3.4
Er	ppm	18.6	13.0	16.3	17.7	15.1	9.8
Tm	ppm	2.5	1.8	2.3	2.4	2.2	1.2
Yb	ppm	14.9	10.9	13.6	14.4	14.0	7.4
Lu	ppm	2.0	1.5	1.9	2.0	2.0	1.1
$(La/Sm)_N$		2.38	2.45	1.98	1.66	3.65	5.65
$(Sm/Yb)_N$		0.51	0.68	0.42	0.43	0.66	3.37
$(Eu/Eu^*)_N$		0.93	0.90	0.63	0.87	0.93	1.05
$(Y/Ho)_N$		1.01	1.03	1.00	1.06	1.02	1.00

$Eu^* = (Sm+Gd)/2$.

In addition, 36 spot analyses of garnet porphyroblasts from the Ekinözü region were conducted to determine their mineral chemistry. The analyses were expressed as weight percentages of oxides, and only data with total oxide contents between 98% and 101% were included in the evaluation. Detailed results are provided in Appendix A. The mineral chemistry of garnets was determined using a JXA-8230 Electron Probe Microanalyzer (EPMA) equipped with wavelength-dispersive spectroscopy (WDS). Three polished and carbon-coated thin sections containing four porphyroblasts from different sampling points were analyzed, and the results were corrected for matrix effects using the ZAF correction software. The EPMA analyses were completed at the YEBİM, Ankara University.

4 Results

4.1 Mineralogical and petrographic characteristics of garnets

The garnet occurrences observed in the study area, located within the Ekinözü district of Kahramanmaraş, have developed as porphyroblasts within schists belonging to the Bitlis-Pötürge-Malatya metamorphic zone. In the field, these schists typically exhibit reddish-yellowish and brownish hues (Figure 3a). With well-developed schistosity planes, these rocks exhibit porphyroblastic textures, characterized by garnet (Figure 3b). From a petrographic perspective, the units are of chlorite-biotite schist composition and exhibit a lepidoblastic texture. Their mineral assemblages are mainly composed of chlorite, biotite, quartz, garnet, and opaque minerals (Figure 3c, d). Biotite minerals in the rock are frequently altered to chlorite, during which opaque mineral inclusions developed along the cleavage planes.

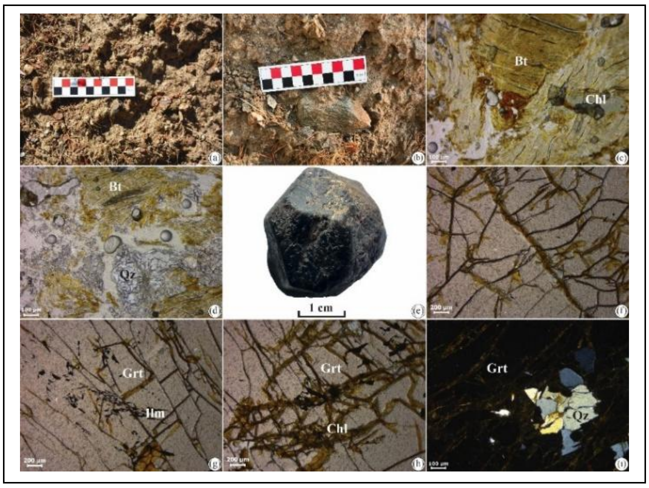

Figure 3. (a), (b): Field appearances of schists containing garnet porphyroblasts from the Ekinözü region. (c), (d): Photomicrographs of chlorite-biotite schists. (d): Fractured and cracked quartz minerals. (e): Image of the pentagonal dodecahedral crystal form of the porphyroblasts; features observed in the porphyroblasts. (f): Fractured-cracked texture. (g): Ilmenite. (h): Chloritization and (ı): Quartz inclusions (Bt: Biotite, Chl: Chlorite, Grt: Garnet, Ilm: Ilmenite, Qz: Quartz).

The garnets observed within the schists exhibit deep red to nearly black colors with vitreous luster, and the porphyroblasts can be physically separated from the host rock with relative ease (Figure 3e). Microscopic investigations revealed that garnet crystals possess an intensely fractured and cracked structure (Figure 3f). Under the polarizing microscope, zones of chloritization accompanied by brown limonitization were identified along the fractures and cracks (Figure 3g, h). Although garnet crystals generally do not show distinct zoning, they contain various mineral inclusions. Among these inclusions, quartz, chlorite, and opaque minerals such as ilmenite and magnetite were identified (Figure 3g-ı).

4.2 Confocal Raman spectroscopy

Confocal Raman Spectroscopy (CRS) is a non-destructive, high-resolution analytical technique widely used in mineralogical and gemological investigations. The advantages of CRS include no special sample preparation prior to analysis, the ability to examine samples while preserving their physical integrity, the provision of high-resolution spectral data, and the capability to produce linear and three-dimensional chemical maps based on measurement points. However, factors such as the degree of alteration of the mineral or structural degradation can negatively affect the Raman signal intensity, thereby limiting the sensitivity of the analysis [25]-[33].

As a result of CRS analyses applied to the Ekinözü garnet porphyroblasts, a total of 11 Raman shift bands with varying intensities were identified. The strongest Raman signals were detected in the ranges of 913-916 cm^{-1} and 342-345 cm^{-1}, while medium-intensity peaks were recorded at 553-555, 496-498, 369-370, and 165-166 cm^{-1}. In addition, lower-intensity signals were observed at 1035-1038, 859-863, 629-630, 474-476, and 213-216 cm^{-1} (Table 2 and Figure 4). In the Raman spectra of the garnet porphyroblasts, strong Raman scattering above 800 cm^{-1} corresponds to the stretching vibrations of bonds between silicon and oxygen atoms.

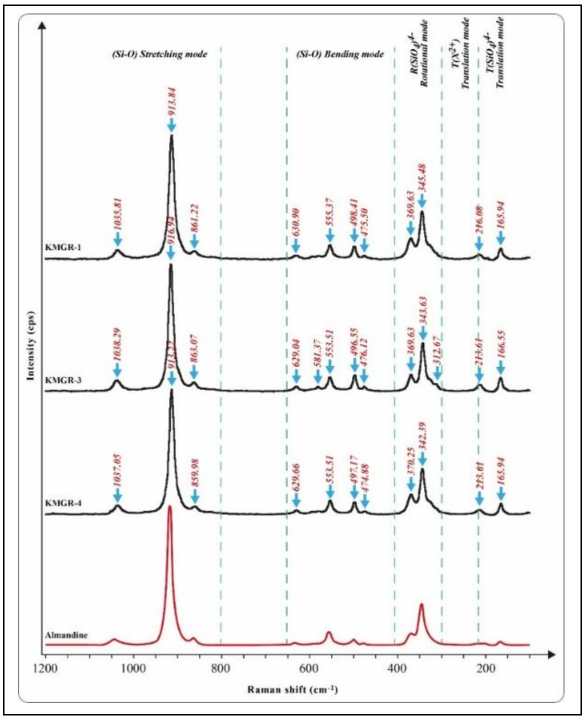

Figure 4. Raman spectra of garnet porphyroblasts from the Ekinözü region and the almandine-type garnet end-member [39].

Table 2. Raman spectral features of standard garnet end-members compared with Ekinözü garnet porphyroblasts [35],[36].

Symmetry	Assigment	Pyrope	Almandine	Grossular	Spessartine	Ekinözü
$T_{2g}+T_{1u}$	ν_3	1062	1032	1007	1027	1035-1038
E_g	ν_3	938	920	904	913	
$T_{2g}+T_{1u}$	ν_3	899	892	850	878	
$T_{2g}+T_{1u}$	ν_3	866	862	826	849	859-863
A_{1g}	ν_1	925	910	881	905	913-916
E_g	ν_1	911	910	852	892	
$T_{2g}+T_{1u}$	ν_4	648	628	629	628	629-630
E_g	ν_4	626	593	590	592	
$T_{2g}+T_{1u}$	ν_4	598	576	577	573	
$T_{2g}+T_{1u}$	ν_4	510	498	509	499	496-498
A_{1g}	ν_2	562	553	549	550	553-555
E_g	ν_2	524	521	526	521	
$T_{2g}+T_{1u}$	ν_2	490	474	478	472	474-476
E_g	ν_2	439	421	416	410	
$T_{2g}+T_{1u}$	$R(SiO_4)$	379	355	383	350	
E_g	$R(SiO_4)$	365	368	369	372	369-370
A_{1g}	$R(SiO_4)$	362	347	374	347	342-345
$T_{2g}+T_{1u}$	$R(SiO_4)$	350	312	349	314	
$T_{2g}+T_{1u}$	$T(M)$	272	212	246	220	213-216
$T_{2g}+T_{1u}$	$T(M)$	208	166	178	173	165-166

Raman signals in the range of 400-650 cm^{-1} are associated with bending modes of the same atomic bonds. Furthermore, medium-intensity Raman bands observed in the range of 300-400 cm^{-1} are attributed to rotational movements of the $(SiO_4)^{-4}$ tetrahedra in the silicate structure. Raman shifts observed between 200-300 cm^{-1} are associated with lattice vibrational modes involving divalent cations, primarily Fe^{+2} and Mg^{+2}, while the low-frequency Raman bands within 100-200 cm^{-1} reflect the collective vibrational modes of the $(SiO_4)^{-4}$ tetrahedra (Figure 4) [34]-[38].

The obtained spectra were compared with CRS data of garnet end-members (almandine, pyrope, spessartine, grossular, and andradite) reported in the literature. The comparison revealed that the Raman spectral data of the Ekinözü garnets show a high degree of similarity, particularly with the almandine end-member (Table 2).

4.3 X-Ray powder diffraction (XRD) analyses

As a result of XRD analyses applied to the host rock powder samples, characteristic diffraction peaks belonging to garnet, quartz, calcite, and chlorite minerals were identified in the chlorite-biotite schist sample (Figure 5).

When the XRD patterns of garnet porphyroblasts collected from different locations within the study area were compared, they showed highly similar patterns and exhibited regular, distinct peaks beginning at approximately $2\theta \approx 15°$. In these patterns, in addition to the peaks corresponding to garnet minerals with almandine-pyrope compositions, reflections belonging to ilmenite, interpreted as inclusion minerals, were also observed (Figure 5). Although a complete compositional separation of the garnets was not possible in the XRD evaluations, it was concluded that the porphyroblasts from the Ekinözü region possess characteristics close to the almandine and pyrope end-members (Table 3).

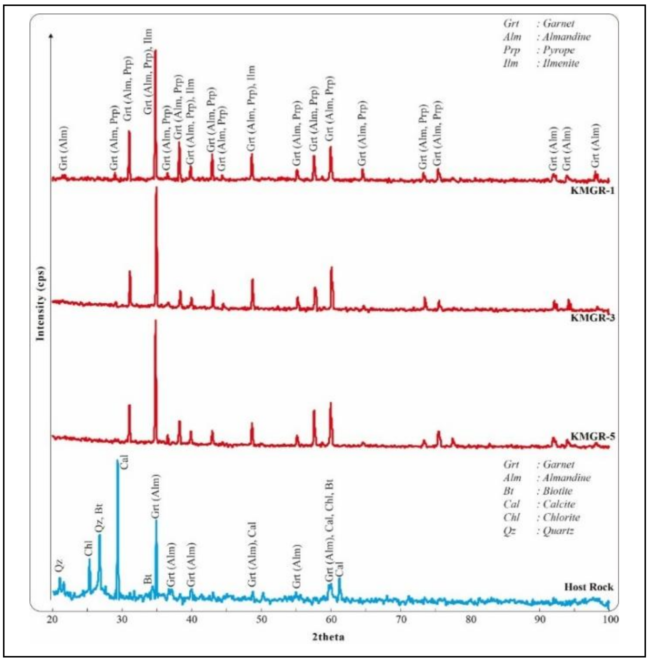

Figure 5. XRD patterns of garnet porphyroblasts and the chlorite-biotite schist host rock.

4.4 Major oxide, trace and REE characteristics of garnets

Whole-rock/crystal analyses of garnet porphyroblasts obtained from the Ekinözü region were evaluated in terms of major element oxides, trace elements, and REE, and the results are presented in Table 1. In garnet porphyroblasts, the Al_2O_3 content ranges between 20.10-20.35 wt.%, SiO_2 between 34.17-35.19 wt.%, MgO between 2.40-2.87 wt.%, Fe_2O_3 between 41.67-42.26 wt.%, TiO_2 between 0.22-0.26 wt.% and CaO between 0.95-1.33 wt.%. The loss on ignition (LOI) was calculated to range between -2.4 and -1.1% (Table 1 and Figure 6).

Table 3. 2θ and d-spacing values of Ekinözü garnet porphyroblasts in relation to garnet end-members [40]-[44].

Pyrope		Spessartine		Almandine		Andradite		Grossular		Ekinözü	
2θ	d	2θ	d	2θ	d	2θ	d	2θ	d	2θ	d
18.90	4.70	18.70	4.76	18.84	4.71					18.90	4.65
29.04	3.07	28.71	3.11	28.95	3.08	29.67	3.01			29.09	3.06
								30.12	2.97		
31.10	2.88	30.73	2.91	31.00	2.88	33.30	2.69			31.05	2.88
		34.46	2.61					33.78	2.65		
34.88	2.57			34.77	2.58	34.91	2.57			34.76	2.58
36.64	2.45					36.52	2.46	37.12	2.42		
38.33	2.35	37.86	2.38	38.21	2.36					38.25	2.35
		39.46	2.28					38.69	2.33		
39.96	2.26			39.83	2.26					39.87	2.26
						40.97	2.20	41.69	2.17		
43.07	2.10	42.52	2.13	42.93	2.11					43.02	2.10
								47.22	1.93		
		48.16	1.89								
48.80	1.87			48.64	1.87					48.70	1.86
								53.50	1.71		
55.33	1.66	54.59	1.68	55.14	1.67	54.88	1.67			55.20	1.66
		57.01	1.62			57.14	1.61				
57.79	1.60			57.60	1.60			58.18	1.59	57.58	1.60
		59.37	1.56							60.00	1.54
73.65	1.29										
		74.66	1.27								
75.79	1.26			75.51	1.26	88.85	1.10			75.51	1.25

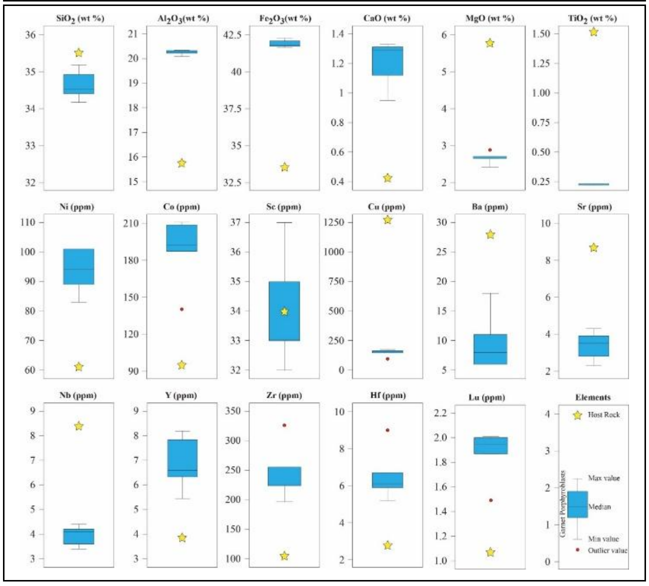

Figure 6. Boxplots of the analyzed major oxides and some trace elements in garnet porphyroblasts and host rock.

With respect to certain trace elements that contribute to color formation and are frequently utilized in petrogenetic interpretations, the Ekinözü garnet porphyroblasts yielded values of 83-101 ppm Ni, 140.2-211 ppm Co, 32-37 ppm Sc, 95.4-176 ppm Cu, 6-8 ppm Ba, 2.3-4.3 ppm Sr, 3.4-4.4 ppm Nb, 128.7-183.9 ppm Y, 196.6-326.1 ppm Zr, 5.2-9 ppm Hf and 1.5-2 ppm Lu (Table 1 and Figure 6).

In the multi-element diagram normalized to the upper continental crust (UCC), the Ekinözü garnet porphyroblasts display depletion trends in Sr, K, Rb, Ba, Nb, and Ti, whereas enrichment up to 10 times is observed in elements such as Th, Ta, Ce, P, Zr, Hf, Sm, Y, and Yb (Figure 7a). In the diagram normalized to the lower continental crust (LCC), enrichments up to 10 times are observed in Ta, P, Zr, Hf, Sm, Y, and Yb, while depletion trends are evident in the other elements (Figure 7b). In the Primitive Mantle (PM)- normalized multi-trace element diagrams, except for Sr, the garnet porphyroblasts show trace-element enrichments ranging from 10 to 100 times (Figure 7c). In the multi-element diagrams normalized to Chondrite, distinct enrichments are observed in Ba, Th, Ta, and P, whereas other trace elements exhibit depletion trends (Figure 7d). The observation of parallel geochemical behaviors in similar elements across all normalized diagrams (UCC, LCC, PM and Chondrite) indicates that the garnet porphyroblasts and the chlorite-biotite schists hosting them were formed through similar petrological processes. Rare earth elements (REE) are a group of elements of strategic importance in energy production technologies and advanced technological material applications. Today, the majority of global REE production is supplied from clay-type deposits located in southern China. Together with yttrium (Y), this group includes the elements between lanthanum (La) and lutetium (Lu) in the periodic table and due to increasing industrial demand, they are considered among the critical raw material resources expected to gain even more importance in the future. In recent years, there has been a notable increase in mining activities of REE-enriched deposits [45],[46].

Evaluation of the REE concentrations of the garnet porphyroblasts from the Ekinözü region reveals that La values range between 15.1-50.2 ppm, Ce between 29.8-91.7 ppm, Pr between 4.0-11.1 ppm, Nd between 16.6-40.4 ppm, Sm between 5.4-8.7 ppm, Eu between 1.7-3.6 ppm, Gd between 11.6-16.7 ppm, Tb between 2.8-3.9 ppm, Dy between 19.7-28.5 ppm, Ho between 4.3-6.3 ppm, Er between 13.0-18.6 ppm, Tm between 1.8-2.5 ppm, Yb between 10.9-14.9 ppm and Lu between 1.5-2.0 ppm (Figure 8). While relatively broad and asymmetric distributions are observed for La, Ce, Nd, Gd, Dy and Er, the distributions of the other REEs appear narrower and more homogeneous. In the chondrite-normalized REE multi-element diagram, it is evident that the Ekinözü garnet porphyroblasts contain high levels of rare earth elements and these concentrations exhibit a distribution pattern of heavy rare earth elements (HREE) similar to that of the chlorite-biotite schist host rock from the same sampling area. However, the host rock is characterized by a stronger LREE enrichment relative to the garnet porphyroblasts. In contrast, the garnet porphyroblasts exhibit similar levels of enrichment in both LREE and HREE (Figure 7e). The total REE contents of the garnet porphyroblasts range between 162.07-284.89 ppm, while the $(Eu/Eu^*)_N$ ratio was calculated as 0.63-0.93, the $(Ce/Ce^*)_N$ ratio as 4.71-8.21 and the $(Y/Ho)_N$ ratio as 1.00-1.06 (Figure 8). The results point to a minor negative Eu anomaly within the garnet porphyroblasts (Figure 7e). When the total REE contents of the Ekinözü garnet porphyroblasts are considered, they fall below the levels of globally economic garnet deposits (Figure 7f).

4.5 Mineral chemistry and geothermometry of garnets

The silicon (Si) contents of the garnets vary between 5.61-6.14 atoms per formula unit (a.p.f.u.). Aluminum (Al^{VI}) ranges between 3.44-4.24, iron (Fe^{+2}) between 4.65-5.75, magnesium (Mg) between 0.46-0.77, manganese (Mn) between 0.01-0.30 and calcium (Ca) between 0.09-0.40 a.p.f.u. The $Fe^{+2}/(Fe^{+2}+Mg)$ ratios of the garnets range from 0.86-0.91, while $Mg/(Mg+Fe^{+2})$ ratios range from 0.09-0.14. The mineral chemistry data are provided in Appendix A.

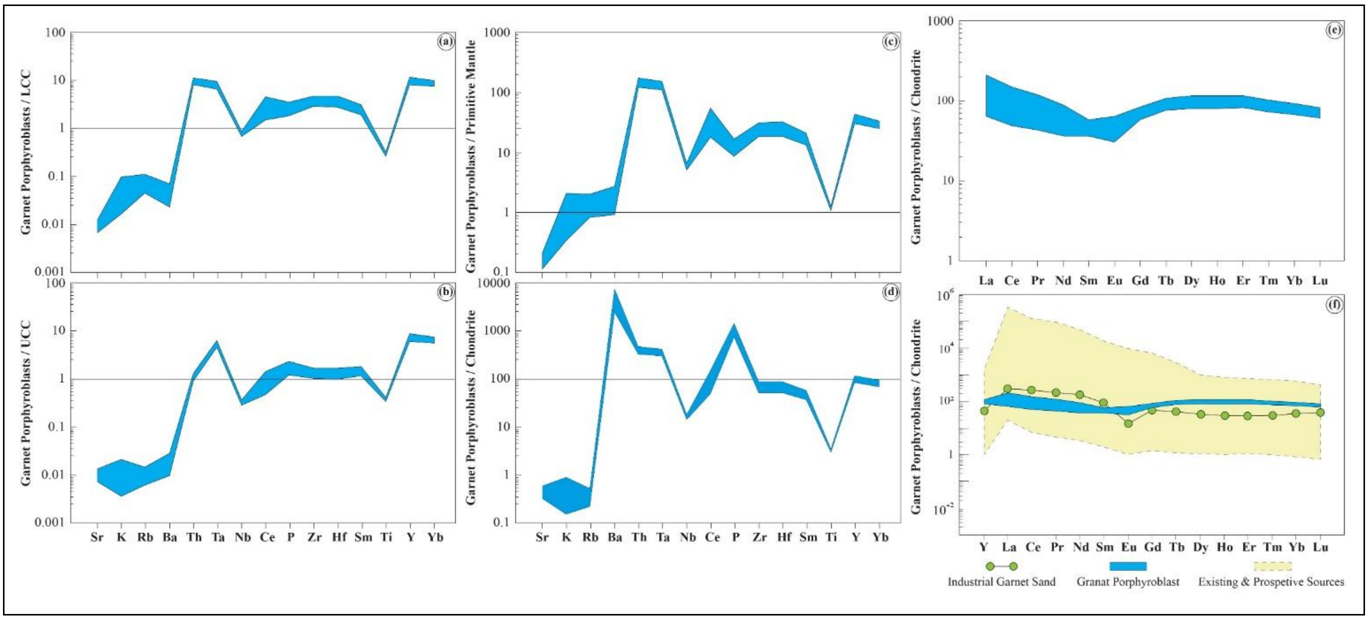

Figure 7. Multi-trace element variation diagrams of Ekinözü garnet porphyroblasts normalized to (a): Lower continental crust [47]. (b): Upper continental crust [47]. (c): Primitive mantle [48], and (d): chondrite values [49]. (e): Chondrite-normalized REE variation diagram [49]. (f): Comparison of chondrite-normalized Y+REE patterns of garnet porphyroblasts with industrial garnet sands and existing Y+REE sources [45],[46].

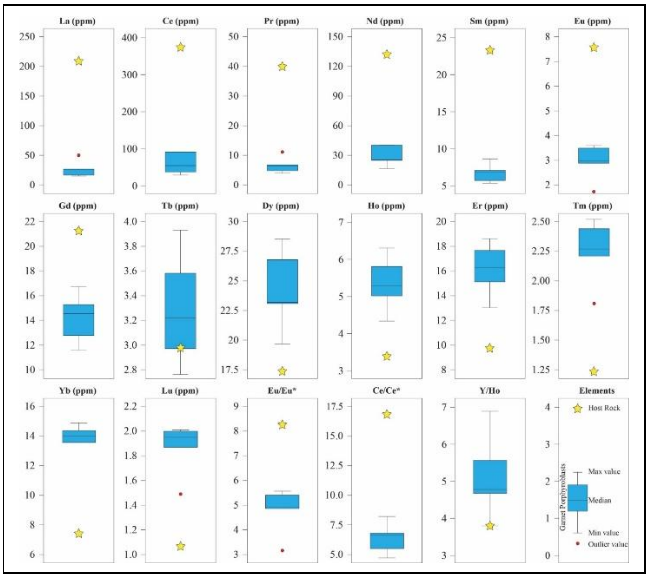

Figure 8. Box-plot diagram showing the REE contents of garnet porphyroblasts from the Ekinözü.

Based on these data, the chemical formula of the Ekinözü garnets were calculated as Alm$_{0.80-0.88}$Prp$_{0.07-0.13}$Grs$_{0.01-0.07}$Sps$_{0.00-0.05}$. In the triangular diagram of end-member compositions defined by Wright (1938), the investigated garnets correspond to the field dominated by almandine composition (Figure 9a). Similarly, in the cation-based classification diagrams developed by Grew et al. (2013), the garnets also plot within the almandine field (Figure 9b). The Ca-Mg-(Fe^{+2}+Mn) and Prp-(Alm+Sps)-Grs triangular diagrams proposed by Wright [50] likewise indicate that the Ekinözü garnets crystallized under medium- to high-grade metamorphic conditions (Figure 9c, d). In this context, the formation of garnets is interpreted as related to regional metamorphic processes in the area.

Geothermobarometry is an important petrographic method that quantitatively determines the temperature and pressure conditions prevailing during the crystallization or recrystallization of magmatic and metamorphic rocks. Geothermometers have been developed primarily based on cation-exchange reactions or chemical equilibrium relationships observed among minerals that change during metamorphism. Although numerous types of geothermometers are employed in petrological studies, the garnet-biotite geothermometer is particularly preferred in medium- to high-grade metamorphic rocks where garnet and biotite minerals coexist. The basis of this method is the mutual exchange of iron (Fe) and magnesium (Mg) cations between garnet and biotite. The equilibrium constant (KD) corresponding to this cation exchange can be calculated from mineral chemistry data, and by relating this constant to various calibration equations, the formation temperatures of the rocks can be estimated. Since the 1970s, garnet-biotite geothermometers have been experimentally and theoretically calibrated by various researchers and are regarded as reliable tools for reconstructing metamorphic conditions. This method, in particular, provides significant contributions to understanding the geodynamic evolution of regions affected by regional metamorphism [52]-[58]. Calculations based on the mineral-chemistry analyses of garnet porphyroblasts from the Ekinözü region indicate formation temperatures ranging from 388.4 °C to 513.9 °C (average 465.4±41.6 °C). Geobarometric evaluations conducted on the same samples suggest that crystallization likely occurred under pressures of approximately 3.8-5.2 kbar (average 4.5 kbar) (Appendix B).

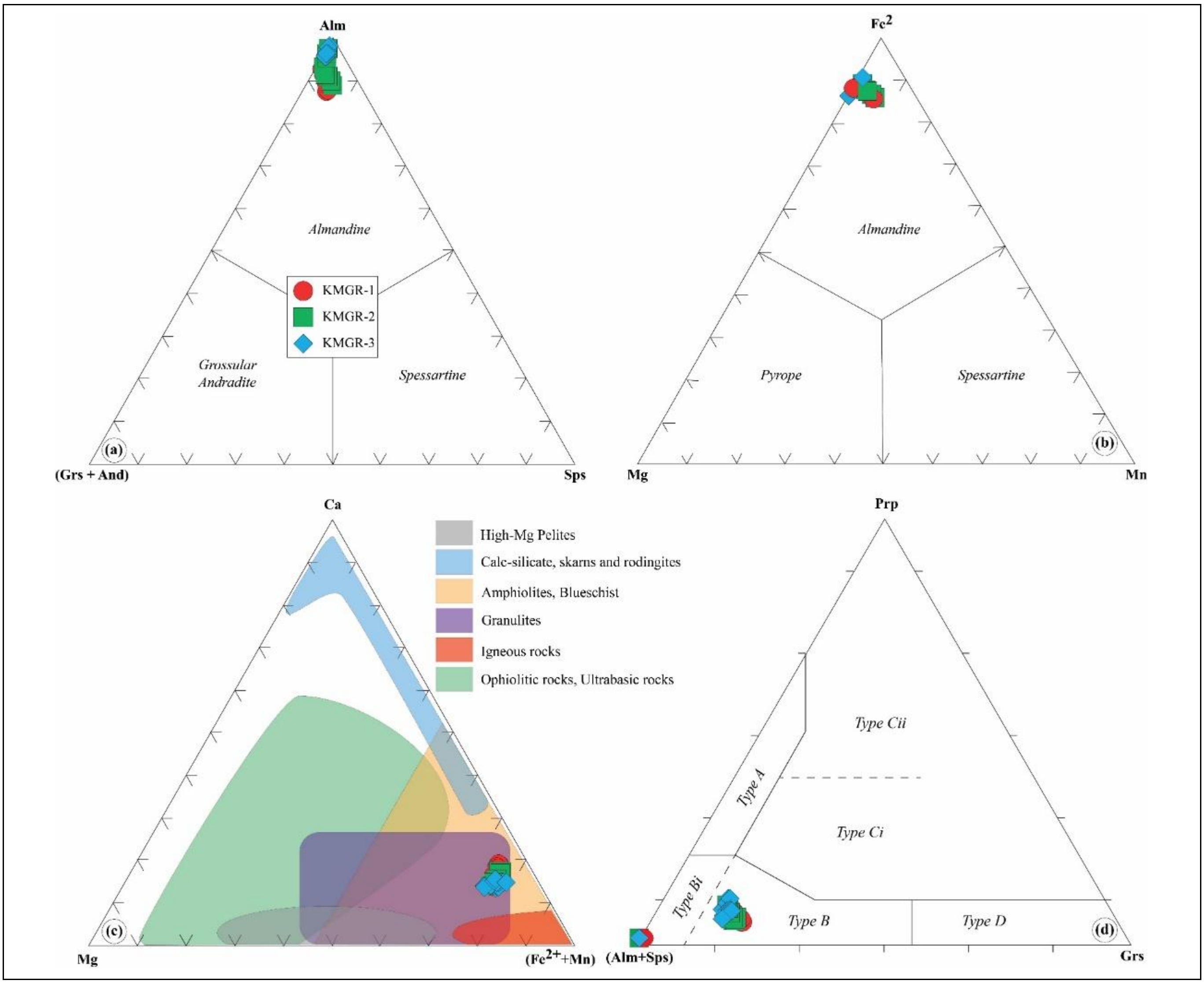

Figure 9. (a): Ternary diagram based on the almandine-(grossular + andradite)-spessartine end-member composition of Ekinözü garnet porphyroblasts [50]. (b): Their positions in the (Mg-Mn-Fe^{2+}) ternary diagram based on cation values [51]. (c): Genetic classification diagram based on Ca-Mg-(Fe^{2+} + Mn) cation contents; and (d): Ternary diagram based on Prp-(Alm + Sps)-Grs end-member compositions [50].

4.6 Scanning Electron Microscopy (SEM) investigations

The surface features of garnet porphyroblasts from the Ekinözü region were examined using SEM, and their gemstone potential was evaluated. Morphologically, these garnets exhibit a pentagonal dodecahedron form and display a vitreous luster in reddish to nearly black tones when cut and polished. In wide-field SEM images, no significant traces of deformation were observed on the crystal surfaces (Figure 10d-f). However, detailed images obtained at higher magnification revealed fractures and cracks (Figure 10f).

These microcracks are interpreted to have formed due to chemical reactions during metamorphism, and secondary quartz minerals were observed to have formed within these voids.

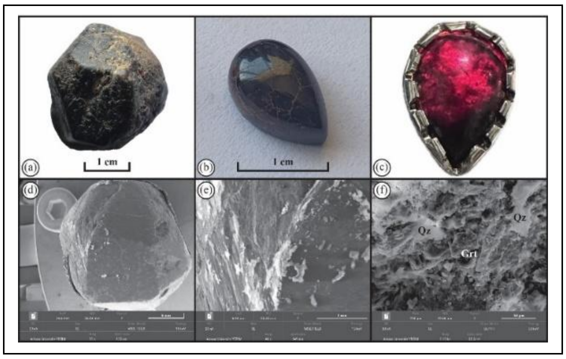

Figure 10. (a): Unprocessed, and (b): Processed hand specimens of Ekinözü garnet porphyroblasts. (c): Illuminated garnet porphyroblast exhibiting an attractive red color. (d)-(f): SEM images at 13x, 58x and 1100x magnifications, respectively.

Based on these findings, it is understood that the investigated garnet porphyroblasts generally do not contain abundant voids but do exhibit a fractured structure, with secondary minerals forming within these cracks. This condition requires that the garnets be evaluated as semi-precious stones rather than as precious gemstones. Nevertheless, it is anticipated that, in the event that crack-free garnet porphyroblasts are obtained through further detailed field and sampling studies in the region, such minerals could yield specimens of precious gemstone quality.

5 Discussion

5.1 Gemological characteristics of garnets

The gemological properties of the garnet porphyroblasts were evaluated using classical and basic testing methods. However, advanced gemological analyses required for a comprehensive assessment of their gemstone characteristics (e.g., FTIR, PIXE, PIGE, UV-Vis-NIR absorption spectroscopy) could not be carried out. Consequently, the interpretations of these data are presented in the discussion section.

Garnet group minerals, with their wide compositional diversity, are important gemstones used in jewelry production, decorative arts, and industrial applications (particularly as abrasives). Within the scope of this study, various gemological analyses were conducted to assess the gemstone potential of garnet porphyroblasts in the Ekinözü Formation. The tests performed included color measurements, specific gravity, refractive index, and optical behavior observed under ultraviolet light.

Color analyses were conducted using the L*a*b* color space, adopted by the International Commission on Illumination (CIE) in 1976 and now a global standard. In this system:

- L* shows lightness (0 = black, 100 = white),
- a* shows red-green axis (+a* = red, -a* = green),
- b * shows yellow-blue axis (+b* = yellow, -b* = blue).

According to the obtained data, the average color values of the Ekinözü garnets were determined as L* = 41.91, a* = 1.21, and b* = 1.80. This color profile indicates that the stones possess dark red tones approaching black.

Based on gemological measurements, the specific gravity of the Ekinözü garnets ranges from 3.84 to 4.15, while their refractive indices range from 1.78 to 1.80. In spectroscopic analyses, the stones exhibited strong absorption bands at 580 nm (yellow band) and moderately intense absorption at 520 nm (green band). In addition, these garnet samples did not exhibit any fluorescence or phosphorescence under UV light.

In comparison with garnet types internationally recognized as gemstones, it was observed that the physical and optical properties of the Ekinözü garnet porphyroblasts show significant similarity to almandine-type garnets (Table 4).

5.2 Coloration mechanism and gemological character

The causes of different colorations within the same mineral remain one of the major questions in the literature. However, color is a characteristic feature directly related to a mineral's chemical composition. In particular, transition metals (Ti, V, Cr, Mn, Fe, Ni, Co and Cu) present in minerals can be the primary cause of coloration [59]-[61]. In this study, Enrichment Factor (EF) values were calculated in order to determine which elements play an important role in color formation. EF is the ratio of the content of an element in a sample to that of the same element in a reference material, and it is calculated as follows:

$$EF = \frac{(Element/Normalizing\ Element)_{Sample}}{(Element/Normalizing\ Element)_{Reference}}$$

EF calculations normalize the measured element content relative to reference elements such as Al, Fe, Mn, or Rb in the sample [62]. In this study, aluminum (Al) was selected as the normalizing element because it is commonly present in the chemical formula of pyralspite subgroup end-members such as pyrope, almandine, and spessartine, and it also occurs in relatively high amounts in the Earth's crust. In addition, the continental crust values proposed by Rudnick and Gao [47] were used as the reference material.

According to the EF values, five different enrichment levels have been defined [62]:

- EF < 2 → negligible or minimum enrichment
- EF = 2-5 → moderate enrichment
- EF = 5-20 → significant enrichment
- EF = 20-40 → very high enrichment
- EF > 40 → extremely high enrichment

The EF values calculated for selected elements, together with the reference material values, are presented in Table 5. In the Ekinözü garnets, Y (5.3-7.6) and Co (4.2-6.2) show significant enrichment, whereas Fe (4.4-4.5), Cu (2.8-5.1), U (1.8-3.2), and Mn (1.6-3.2) display moderate enrichment. In addition, Ce, Zr, Ti, V, Ni, and Cr exhibit negligible enrichment (Table 5). Based on these results, the red to reddish-black colors of the Ekinözü garnets are most likely related to the enrichment of Co, Fe, U, and Mn. However, to precisely determine the cause of coloration, highly sensitive atomic-scale analyses are required. Optical absorption spectrometry analyses performed during the gemological tests also revealed peaks at 520 nm and 580 nm, which clearly indicate the important role of Fe^{+2} ions in color formation [63]. Moreover, EPMA data also demonstrate the high concentration of Fe^{+2} (4.65-5.75 a.p.f.u.). Gemological investigations also demonstrate that the garnets display a vitreous luster on their pentagonal dodecahedron crystal faces and exhibit optical characteristics ranging from transparent to semi-transparent. With these qualities, garnets are considered suitable for jewelry design. The gemstones can be faceted or cabochon-cut. In this study, the garnets were cut into drop-shaped cabochons and transformed into jewelry with silver using traditional goldsmithing techniques (Figure 11). As a result, it is evaluated that the garnet porphyroblasts obtained from the Ekinözü region have the potential to be utilized as gemstones. In particular, their dark red color and transparency indicate that, when processed, they can provide both economic and aesthetic value (Figure 10a-c).

Table 4. Gemological comparison of Ekinözü garnets and end-members [59].

Granat Types	Refractive Index	Specific Gravity	Color	Optic Absorption Spectra
Grossular	1.730-1.760	3.57-3.76	Green through reddish orange and colorless	Blue: 440 and 450 nm; Green: 500 nm
			Yellow, orange	Purple: 418 nm; Blue: 434 and 489 nm; Green: 503 and 529 nm
Andradite	1.880-1.895	3.80-3.90	Very slightly yellowish green through orange yellow	Blue: 443 nm (strong)
				Blue: 464, 485 (Topazolite)
				Blue: 443 nm (Demantoide); Orange: 622, 640 nm, Red: 693, 701 nm
Pyrope	1.714-<1.742	3.62-3.87	Purplish red through reddish orange and colorless	Yellow: 575 nm (strong); Green: 505, 527 nm (strong)
Pyrope-Almandine	1.742-<1.785	3.74-3.94	Reddish orange through red purple	-
Almandine	1.785-1.830	3.85-4.30	Orange red through purplish red	Yellow: 576 nm (strong); Green: 526, 505 nm (strong); Orange: 617 nm (weak); Blue: 462 nm (weak)
Almandine-Spessartine	1.810-1.820	4.12-4.28	Reddish orange through orange red	-
Spessartine	1.780-<1.810	4.12-4.25	Yellowish orange through reddish orange	Blue: 430, 461 and 485 nm (strong) 462 nm (medium); 489 nm (very weak); Green: 495 nm (weak); Purple: 424 nm (weak)
Pyrope-Spessartine	1.742-<1.780	3.62-4.33	Greenish yellow through purple	-
Ekinözü Garnets	1.78-.1.80	3.84-4.15	Glassy dark red-black	Yellow: 580 nm (strong); Green: 520 nm (medium)

Table 5. Calculated Enrichment Factors for selected elements and reference materials [47].

Selected Elements	KMGR-1	KMGR-2	KMGR-3	KMGR-4	KMGR-5	Continental Crust (ppm)
U	2.3	2.3	1.8	3.0	3.2	1.3
Mn	3.2	2.5	1.6	2.6	2.3	774
Y	7.6	5.3	6.3	7.3	6.0	19
Co	5.5	5.7	4.2	6.2	6.1	26.6
Fe	4.4	4.4	4.5	4.4	4.4	52180
Ce	1.0	1.0	0.7	0.5	1.7	43
Zr	1.3	1.3	1.2	1.9	1.5	132
Ti	0.2	0.3	0.3	0.0	0.2	4316
V	0.1	0.1	0.2	0.1	0.1	138
Ni	1.2	1.2	1.1	1.3	1.3	59
Cu	4.8	4.6	4.2	2.8	5.1	27
Cr	0.3	0.3	0.4	0.2	0.3	135

Figure 11. A silver jewelry set produced using garnet porphyroblasts from the Ekinözü region [64].

6 Conclusions

Comprehensive analyses of the gemological, mineralogical, petrographic, geochemical, and spectroscopic features of garnet porphyroblasts from the Ekinözü region have revealed the following results:

1. The studied garnet porphyroblasts display hues from dark red to nearly black and vary in size from 0.5 to 4 cm, exhibit a pentagonal dodecahedron crystal morphology, and were observed within high-grade metamorphosed schists.
2. Formed through regional metamorphism and subsequent deformation, the porphyroblasts are commonly fractured, occasionally cracked, and contain inclusions. Within the garnet crystals, inclusions of quartz, chlorite, and opaque minerals such as ilmenite and magnetite are common, while chlorite and limonite alterations were observed along cracks,
3. X-ray diffraction (XRD) patterns indicate that the garnets are predominantly of almandine-pyrope composition. However, due to slight variations in crystal structures, XRD data alone are not sufficient to precisely distinguish the garnet species,
4. Confocal Raman spectroscopy (CRS) results revealed that the characteristic Raman peaks of the garnet crystals are highly consistent with almandine. These spectral data, supported by mineral chemistry and XRD results, confirm that the garnets are predominantly of almandine composition,
5. According to mineral chemistry data, the garnets are of almandine composition ($Alm_{0.80-0.88}Prp_{0.07-0.13}Grs_{0.01-0.07}Sps_{0.00-0.05}$). Geothermometric calculations based on garnet-biotite pairs indicate crystallization temperatures ranging between approximately 388.4-513.9 °C (average 465.4 ± 41.6 °C). These values correspond to greenschist facies conditions and provide insights into the metamorphic temperature levels in the region,
6. Geochemical analyses show that the Ekinözü garnet porphyroblasts exhibit depletion in trace elements such as Sr, K and Rb, while displaying enrichment in elements such as Th, Ta, P, Y and Yb. REE analyses indicate that the garnet samples exhibit enrichment of both heavy and light rare earth elements (HREE-LREE) of up to nearly 100 times. The total REE contents of the Ekinözü garnet porphyroblasts range between 162.07-284.89 ppm, values that fall below those of globally economic garnet deposits,
7. According to the Enrichment Factor (EF) calculated from chemical analyses, Co, Fe, U and Mn elements play a significant role in coloration. Furthermore, EPMA analyses and optical absorption spectroscopy support the presence of high amounts of Fe^{+2} ions,
8. The examined garnet porphyroblasts display a vitreous luster on their pentagonal dodecahedron crystal faces and exhibit optical properties ranging from transparent to semi-transparent. SEM investigations revealed the presence of microcracks within the garnets, where secondary mineral formations occur. This indicates that the Ekinözü garnets should be classified as semi-precious gemstones. The garnets from Ekinözü were processed into jewelry by applying the cabochon technique, which is commonly used for semi-precious stones and produced an appealing appearance. It is considered that with the continuation of detailed research in the region, crack-free specimens may be discovered, yielding garnets that fall into the category of precious gemstones.

7 Acknowledgment

The authors sincerely thank the Pamukkale University Scientific Research Projects Coordination Unit (PAUBAP) administrators and staff for their support within the scope of the doctoral thesis project numbered 2021FEBE056, on which this paper-presented as an oral presentation at the 10th Geochemistry Symposium-is based. The authors also extend their gratitude to the reviewers for their constructive comments during the evaluation process, to Prof. Dr. Yusuf Kağan Kadıoğlu and Assoc. Prof. Dr. Kıymet Deniz Yağcıoğlu from Ankara University Earth Sciences Application and Research Center (YEBİM) for their assistance in the Confocal Raman Spectroscopy and Mineral Chemistry studies, and to Mustafa Kemal Koca for his help during the fieldwork.

8 Author contribution statements

In the present study, Ufuk Ören contributed to field observations and sample collection, sample preparation for analyses, EPMA and Raman (CRS) analyses, as well as gemological tests. Tamer Koralay contributed to the conception of the study, petrographic examinations, XRD and ICP-MS analyses, evaluation of the results, supervision of the writing, and overall content review of the manuscript.

9 Ethics committee approval and conflict of interest statement

"There is no need to obtain permission from the ethics committee for the article prepared". "There is no conflict of interest with any person / institution in the article prepared".

10 References

[1] Stockton CM, Manson DV. "A proposed new classification for gem-quality garnets". *Gems & Gemology*, 21(4), 205-218, 1985.

[2] Deer WA, Howie RA, Zussman J. *An Introduction to the Rock Forming Minerals*. 2nd ed. London, England, Longman, 1992.

[3] King RJ. "Minerals explained 26: The garnets". *Geology Today*, 15(1), 34-37, 1999.
[4] Wehlus T, Körner T, Leitenmeier S, Heinrich A, Stritzker B. "Magneto-optical garnets for integrated optoelectronic devices". *Physica Status Solidi (a)*, 208(2), 252-263, 2011.
[5] Baxter EF, Caddick MJ, Ague JJ. "Garnet: common mineral, uncommonly useful". *Elements*, 9(6), 415-419, 2013.
[6] Baxter EF, Caddick MJ, Dragovic B. "Garnet: a rock-forming mineral petrochronometer". *Reviews in Mineralogy and Geochemistry*, 83, 469-533, 2017.
[7] Klein C, Philpotts A. *Earth Materials: Introduction to Mineralogy and Petrology*. 2nd ed. Cambridge, England, Cambridge University Press, 2017.
[8] Koralay T, Ören U. "Determination of spectroscopic features and gemstone potential of garnet crystals from the Çamköy region (Aydın - SW Turkey) using XRPD, XRF, Confocal Raman Spectroscopy, EPMA and gemological test methods". *Periodico di Mineralogia*, 89, 105-123, 2020.
[9] Yavuz F, Yıldırım DK. "WinGrt, a Windows program for garnet supergroup minerals". *Journal of Geosciences*, 65, 71-95, 2020.
[10] Liang P, Zhang Y, Xie Y. "Chemical composition and genesis implication of garnet from the Laoshankou Fe-Cu-Au deposit, the northern margin of East Junggar, NW China". *Minerals*, 11(3), 334, 2021.
[11] International Gem Society. "Garnet Symbolism". https://www.gemsociety.org/article/garnet-symbolism-legends/(04.05.2022).
[12] Ören U, Koralay T. "Evaluation of garnet phenocrysts in volcanic rocks (Görece/İzmir - Western Türkiye) for their usability as a semi-precious gemstone by multi-analytical methods". *Spectroscopy Letters*, 57(7), 388-411, 2024.
[13] Perinçek D, Kozlu H. "Stratigraphy and structural relation of the units in the Afşin-Elbistan-Doğanşehir region". *International Symposium on the Geology of the Taurus Belt*, Ankara, Türkiye, 26-29 September 1983.
[14] Bedi Y, Usta D, Özkan MK, Beyazpirinç M, Yıldız H, Yusufoğlu H. "Doğu Toroslar'da (Göksun-Sarız-Elbistan) allokton istiflerin tektono-stratigrafik özellikleri". *58. Türkiye Jeoloji Kurultayı*, Ankara, Türkiye, 11-15 April 2005.
[15] Yılmaz Y, Gürpınar O, Kozlu H, Gül MA, Yiğitbaş E, Yıldırım M, Genç ŞC, Keskin M. Türkiye Petrolleri Anonim Ortaklığı. "Maraş kuzeyinin jeolojisi (Andırın-Berit-Engizek-Nurhak-Binboğa Dağları)". Ankara, Türkiye, 2028, 1987 (unpublished).
[16] Önalan M. "Kahramanmaraş Tersiyer kenar havzasının jeolojik evrimi". *Türkiye Jeoloji Kurultayı Bülteni*, 31, 1-10, 1988.
[17] Genç ŞC, Yiğitbaş E, Yılmaz Y. "Berit metaofiyolitinin jeolojisi". A. *Suat Erk Jeoloji Sempozyumu*, Ankara, Türkiye, 2-5 September 1991.
[18] Baydar O, Yergök AF. "Güneydoğu Anadolu-Kenar Kıvrım Kuşağı-Amanos Dağları Kuzeyi ve Doğu Torosların jeolojisi". Jeoloji Etütleri Dairesi, Ankara, 90 p., 1996 (unpublished).
[19] Yılmaz Y, Yiğitbaş E, Genç ŞC, Şengör AMC. *Geology and Tectonic Evolution of the Pontides*. Editor: Robinson AG. Regional and petroleum geology of the Black Sea and surrounding region, 183-226, Oklahoma, USA, AAPG Memoir, 1997.
[20] Yümün Z, Kiliç A. "Kamandağı ile Camdere köyü arasının stratigrafisi". Cumhuriyet Üniversitesi *Mühendislik Fakültesi Dergisi Seri A - Yerbilimleri*, 19(2), 16-24, 2002.
[21] Candan O, Çetinkaplan M, Topuz G, Koralay OE, Oberhänslı R, Yiğitbaş E, Li Q. "Berit yöresindeki (Kahramanmaraş) eklojit-granat piroksenitlere ait ön bulgular". *65. Türkiye Jeoloji Kurultayı*, Ankara, Türkiye, 2-6 Nisan 2012.
[22] Yalçın C. Çağlayancerit (Kahramanmaraş) Batısının Tektono-Stratigrafisi ve Yapısal Evrimi. MSc Thesis, Kahramanmaraş Sütçü İmam University, Kahramanmaraş, Türkiye, 2012.
[23] Hozatlıoğlu D, Bozkaya Ö, Yalçın H, Yılmaz H. "Göksun, Afşin ve Ekinözü (Kahramanmaraş) bölgesinde yüzeylenen metamorfik masiflerin minerolojik karakteristikleri". *MTA Journal*, 162, 105-146, 2020.
[24] Stockton CM, Manson DV. "Scanning electron microscopy in gemology". *Gems & Gemology*, 17(2), 72-79, 1981.
[25] McMillan PF. "Raman spectroscopy in mineralogy and geochemistry". *Annual Review of Earth and Planetary Sciences*, 17, 225-283, 1989.
[26] Frost R, Kloprogge T, Schmidt J. "Non-destructive identification of minerals by Raman microscopy". *Journal of Internet Vibrational Spectroscopy*, 3, 1-13, 1999.
[27] Hope GA, Woods R, Munce CG. "Raman microprobe mineral identification". *Minerals Engineering*, 14, 1565-1577, 2001.
[28] Mayo DW, Miller FA, Hannah RW. *Course Notes on the Interpretation of Infrared and Raman Spectra*. Hoboken, NJ, USA, John Wiley & Sons, 2004.
[29] Fritsch E, Rondeau B, Hainschwang T, Karampelas S. *Raman Spectroscopy Applied to Gemmology*. Editors: Dubessy J, Caumon M-C, Rull F. Raman Spectroscopy Applied to Earth Sciences and Cultural Heritage, 455-489, Middlesex, United Kingdom, Mineralogical Society of Great Britain & Ireland 2012.
[30] Güllü B, Kadıoğlu YK. "Use of tourmaline as a potential petrogenetic indicator in the determination of host magma: CRS, XRD and PED-XRF methods". *Spectrochimica Acta Part A: Molecular and Biomolecular Spectroscopy*, 183, 68-74, 2017.
[31] Akçe MA, Kadıoğlu YK. "Raman spektroskopisinin ilkeleri ve mineral tanımlamalarında kullanılması". *Nevşehir Bilim ve Teknoloji Dergisi*, 9(2), 99-115, 2020.
[32] Koralay T, Ören U. "Determination of spectroscopic features and gemstone potential of garnet crystals from the Çamköy region (Aydın - SW Turkey) using XRPD, XRF, Confocal Raman spectroscopy, EPMA and gemological test methods". *Periodico di Mineralogia*, 89, 105-123, 2020.
[33] Deniz K. "Mica Types as indication of magma nature, Central Anatolia, Turkey" *Acta Geologica Sinica*, 96(3), 844-857, 2022.
[34] Moore RK, White WB, Long TV. "Vibrational spectra of the common silicates: I. the garnets". *American Mineralogist*, 56, 54-71, 1971.
[35] Hofmeister AM, Chopelas A. "Vibrational spectroscopy of end-member silicate garnets". *Physics and Chemistry of Minerals*, 17, 503-526, 1991.
[36] Kolesov BA, Geiger CA. "Raman spectra of silicate garnets". *Physics and Chemistry of Minerals*, 25, 142-151, 1998.
[37] Bersani D, Lottici P.P. "Applications of Raman Spectroscopy to Gemology". *Analytical and Bioanalytical Chemistry*, 397, 2631-2646, 2010.

[38] Jenkins A.L., Larsen R.A. "Gemstone Identification Using Raman Spectroscopy". *Spectroscopy*, 19(4), 20-25, 2004.
[39] RRUFF. "Database of Raman spectroscopy". http://rruff.info/almandine/R060099 (15.07.2022).
[40] RRUFF. "Database of X-ray diffraction". http://rruff.info/repository/sample_child_record_powder/by_minerals/Almandine__R060099-9__Powder__DIF_File__10051.txt (12.12.2019).
[41] RRUFF. "Database of X-ray diffraction". https://rruff.info/repository/sample_child_record_powder/by_minerals/Andradite__R060326-9__Powder__Xray_Data_XY_Processed__4295.txt (12.12.2019).
[42] RRUFF. "Database of X-ray diffraction". http://rruff.info/repository/sample_child_record_powder/by_minerals/Grossular__R040066-1__Powder__DIF_File__3313.txt (12.12.2019).
[43] RRUFF. "Database of X-ray diffraction". http://rruff.info/repository/sample_child_record_powder/by_minerals/Pyrope__R100153-9__Powder__DIF_File__11226.txt (12.12.2019).
[44] RRUFF. "Database of X-ray diffraction". http://rruff.info/repository/sample_child_record_powder/by_minerals/Spessartine__R060177-1__Powder__DIF_File__6682.txt (12.12.2019).
[45] Klimpel F, Bau M, Graupner T. "Potential of garnet sand as an unconventional resource of the critical high-technology metals scandium and rare earth elements". *Scientific Reports*, 11, 5306, 2021.
[46] Zirakparvar NA. "Industrial garnet as an unconventional heavy rare earth element resource: Preliminary insights from a literature survey of worldwide garnet trace element concentrations". *Ore Geology Reviews*, 148, 2022.
[47] Rudnick RL, Gao S. *Composition of the Continental Crust*. Editor: Rudnick RL. Treatise on Geochemistry, 1-64, Devon, United Kingdom, Elsevier, 2004.
[48] McDonough WF, Sun S. "The composition of the Earth". *Chemical Geology*, 120, 223-253, 1995.
[49] Evensen NM, Hamilton PJ, O'Nions RK. "Rare earth abundances in chondritic meteorites". *Geochimica et Cosmochimica Acta*, 42, 1199-1212, 1978.
[50] Wright WI. "The composition and occurrence of garnets". *American Mineralogist*, 23, 436-449, 1938.
[51] Grew ES, Locock AJ, Mills SJ, Galuskina IO, Galuskin EV, Hålenius U. "Nomenclature of the garnet supergroup". *American Mineralogist*, 98(4), 785-811, 2013.
[52] Thompson AB. "Mineral reactions in pelitic rock. II. Calculation of some P-T-X (Fe-Mg) phase reactions". *American Journal of Science*, 276, 425-454, 1976.
[53] Holdaway MJ, Lee SM. "Fe-Mg cordierite stability in high-grade pelitic rocks based on experimental, theoretical and natural observations". *Contributions to Mineralogy and Petrology*, 63(2), 175-198, 1977.
[54] Ferry JM, Spear FS. "Experimental calibration of the partitioning of Fe and Mg between biotite and garnet". *Contributions to Mineralogy and Petrology*, 66, 113-117, 1978.
[55] Hodges KV, Spear FS. "Geothermometry, geobarometry and the Al2SiO5 triple point at Mt. Moosilauke, New Hampshire". *American Mineralogist*, 67, 1118-1134, 1982.
[56] Perchuk LL, Lavrenteva IV. *Experimental Investigation of Exchange Equilibria in the System Cordierite-Garnet-Biotite*. Editor: Saxena SK. Kinetics and Equilibrium in Mineral Reactions. Advances in Physical Geochemistry, 199-239, New York, USA, Springer, 1983.
[57] Dasgupta S, Sengupta P, Guha D, Fukuoka M. "A refined garnet-biotite Fe-Mg exchange geothermometer and its application in amphibolites and granulites". *Contributions to Mineralogy and Petrology*, 109, 130-137, 1991.
[58] Bhattacharya A, Mohanty L, Maji A, Sen SK, Raith M. "Non-ideal mixing in the phlogopite-annite binary: Constraints from experimental data on the Mg-Fe partitioning and a reformulation of the biotite-garnet thermometer". *Contributions to Mineralogy and Petrology*, 111, 87-93, 1992.
[59] O'Donoghue M. *Gems: Their Sources, Descriptions and Identification*. Oxford, England, Elsevier, 2006.
[60] Rossman GR. "The geochemistry of gems and its relevance to gemology: Different traces, different price". *Elements*, 5(3), 159-162, 2009.
[61] Galoisy L. "Garnets: From stone to star". *Elements*, 9, 453-456, 2013.
[62] Barbieri M. "The importance of enrichment factor (EF) and geoaccumulation index (IGEO) to evaluate the soil contamination". *Journal of Geology & Geophysics*, 5, 237-240, 2016.
[63] Schmetzer K, Hainschwang T, Kiefert L, Bernhardt HJ. "Pink to pinkish orange malaya garnets from Bekily, Madagascar". *Gems & Gemology*, 37(4), 296-308, 2001.
[64] Ören U. Türkiye'de Seçili Granatların Mineralojik, Petrografik, Spektroskopik, Jeokimyasal ve Gemolojik Özelliklerinin Belirlenmesi. PhD Thesis, Pamukkale University, Denizli, Türkiye, 2023.

Appendix A

Appendix A. Mineral chemistry analysis results and end-member compositions of the Ekinözü garnet porphyroblasts.

Sample	KMGR1.1	KMGR1.2	KMGR1.3	KMGR1.4	KMGR1.5	KMGR1.6	KMGR1.7	KMGR1.8	KMGR1.9
SiO_2	37.38	37.60	37.56	37.97	37.97	37.32	37.99	37.63	37.31
FeO	35.00	35.50	34.95	34.63	35.06	35.30	36.00	36.40	36.47
Al_2O_3	21.13	21.90	21.46	21.76	21.43	21.50	21.74	21.57	21.37
CaO	2.07	2.15	2.32	2.10	1.96	2.01	1.87	1.89	1.70
MgO	2.04	1.95	1.94	2.03	2.00	2.10	2.12	2.10	2.24
MnO	2.12	2.07	1.99	2.09	2.06	1.69	1.08	1.04	0.63
TiO_2	0.06	0.08	0.07	0.03	0.12	0.06	0.12	0.03	0.03
Total	99.79	101.25	100.30	100.61	100.61	99.97	100.91	100.66	99.75
TSi	6.06	6.01	6.06	6.10	6.11	6.04	6.09	6.05	6.05

Appendix A. continued.

Sample	KMGR1.1	KMGR1.2	KMGR1.3	KMGR1.4	KMGR1.5	KMGR1.6	KMGR1.7	KMGR1.8	KMGR1.9
Formula on the basis of 24 oxygen									
Fe^{+2}	4.75	4.75	4.72	4.65	4.72	4.78	4.82	4.89	4.94
Al^{VI}	4.04	4.12	4.08	4.12	4.06	4.10	4.10	4.08	4.08
Ca	0.36	0.37	0.40	0.36	0.34	0.35	0.32	0.33	0.30
Mg	0.49	0.46	0.47	0.49	0.48	0.51	0.51	0.50	0.54
Mn	0.29	0.28	0.27	0.29	0.28	0.23	0.15	0.14	0.09
TAl	0.00	0.00	0.00	0.00	0.00	0.00	0.00	0.00	0.00
Ti	0.01	0.01	0.01	0.00	0.02	0.01	0.01	0.00	0.00
End-member compositions									
Alm	80.60	81.00	80.54	80.44	81.10	81.47	83.22	83.46	84.26
Grs	6.07	6.27	6.82	6.21	5.73	5.94	5.42	5.51	5.04
Prp	8.37	7.92	7.98	8.40	8.25	8.65	8.74	8.57	9.23
Sps	4.93	4.79	4.65	4.93	4.84	3.94	2.53	2.41	1.46
Uv	0.03	0.02	0.01	0.03	0.08	0.00	0.11	0.05	0.00

Sample	KMGR1.10	KMGR1.11	KMGR1.12	KMGR1.13	KMGR2.1	KMGR2.2	KMGR2.3	KMGR2.4	KMGR2.5
SiO_2	37.02	37.54	37.50	37.70	37.61	37.56	37.00	37.68	36.97
FeO	37.11	37.11	37.04	37.58	35.69	35.97	36.34	36.31	36.83
Al_2O_3	21.42	21.34	21.61	21.51	21.58	21.81	21.25	21.56	21.26
CaO	1.46	1.13	1.13	0.79	1.70	1.67	1.66	1.74	1.53
MgO	2.47	2.54	2.57	2.81	1.97	2.05	2.14	2.16	2.14
MnO	0.38	0.34	0.34	0.09	2.21	1.89	1.45	1.13	0.67
TiO_2	0.10	0.07	0.07	0.05	0.03	0.05	0.07	0.06	0.06
Total	99.94	100.06	100.26	100.52	100.78	101.00	99.91	100.63	99.46
Formula on the basis of 24 oxygen									
TSi	5.99	6.06	6.04	6.06	6.05	6.02	6.00	6.06	6.02
Fe^{+2}	5.02	5.01	4.99	5.05	4.80	4.82	4.93	4.88	5.02
Al^{VI}	4.07	4.06	4.10	4.07	4.09	4.12	4.05	4.08	4.08
Ca	0.25	0.20	0.20	0.14	0.29	0.29	0.29	0.30	0.27
Mg	0.60	0.61	0.62	0.67	0.47	0.49	0.52	0.52	0.52
Mn	0.05	0.05	0.05	0.01	0.30	0.26	0.20	0.15	0.09
TAl	0.01	0.00	0.00	0.00	0.00	0.00	0.00	0.00	0.00
Ti	0.01	0.01	0.01	0.01	0.00	0.01	0.01	0.01	0.01
End-member compositions									
Alm	84.80	85.46	85.31	86.04	81.84	82.35	83.06	83.42	85.10
Grs	4.23	3.24	3.32	2.31	4.99	4.87	4.74	5.12	4.54
Prp	10.05	10.42	10.57	11.45	8.04	8.36	8.73	8.84	8.81
Sps	0.88	0.80	0.79	0.21	5.13	4.39	3.35	2.62	1.56
Uv	0.04	0.08	0.01	0.00	0.00	0.03	0.12	0.00	0.00

Sample	KMGR2.6	KMGR2.7	KMGR2.8	KMGR3.1	KMGR3.2	KMGR3.3	KMGR3.4	KMGR3.5	KMGR3.6
SiO_2	37.28	37.18	37.40	35.41	37.51	38.42	37.98	37.93	37.37
FeO	37.09	37.17	37.40	40.13	37.19	37.57	37.03	37.43	37.15
Al_2O_3	21.34	21.51	21.28	21.47	21.70	22.92	21.85	21.92	21.76
CaO	1.05	0.84	0.59	0.91	0.81	0.83	0.95	0.80	0.94
MgO	2.43	2.66	2.90	2.36	2.46	2.51	2.60	2.51	2.61
MnO	0.43	0.33	0.14	0.33	0.38	0.38	0.35	0.38	0.34
TiO_2	0.08	0.06	0.06	0.10	0.07	0.12	0.04	0.09	0.07
Total	99.70	99.74	99.77	100.70	100.12	102.74	100.79	101.05	100.23
Formula on the basis of 24 oxygen									
TSi	6.05	6.02	6.05	5.72	6.06	6.03	6.08	6.07	6.02
Fe^{+2}	5.03	5.04	5.06	5.42	5.02	4.94	4.96	5.01	5.01
Al^{VI}	4.08	4.10	4.06	3.80	4.13	4.24	4.12	4.13	4.13
Ca	0.18	0.15	0.10	0.16	0.14	0.14	0.16	0.14	0.16
Mg	0.59	0.64	0.70	0.57	0.59	0.59	0.62	0.60	0.63
Mn	0.06	0.05	0.02	0.05	0.05	0.05	0.05	0.05	0.05
TAl	0.00	0.00	0.00	0.28	0.00	0.00	0.00	0.00	0.00
Ti	0.01	0.01	0.01	0.01	0.01	0.01	0.00	0.01	0.01

Appendix A. continued.

Sample	KMGR2.6	KMGR2.7	KMGR2.8	KMGR3.1	KMGR3.2	KMGR3.3	KMGR3.4	KMGR3.5	KMGR3.6
				End-member compositions					
Alm	85.86	85.80	86.03	87.57	86.48	86.40	85.66	86.43	85.70
Grs	3.09	2.49	1.74	2.54	2.37	2.43	2.80	2.34	2.77
Prp	10.02	10.94	11.90	9.16	10.21	10.29	10.72	10.31	10.73
Sps	1.00	0.77	0.33	0.73	0.89	0.87	0.82	0.89	0.80
Uv	0.03	0.00	0.00	0.00	0.05	0.01	0.00	0.03	0.00
Sample	**KMGR3.7**	**KMGR3.8**	**KMGR3.9**	**KMGR3.10**	**KMGR3.11**	**KMGR3.12**	**KMGR3.13**	**KMGR3.14**	**KMGR3.15**
SiO_2	37.07	38.22	36.39	38.27	37.03	37.94	36.96	38.31	37.69
FeO	36.68	36.53	44.63	36.64	36.65	36.92	36.34	36.07	36.57
Al_2O_3	21.56	22.26	21.13	21.85	21.33	21.86	21.64	22.11	21.86
CaO	1.03	1.05	0.97	1.00	0.74	0.53	0.52	0.55	0.50
MgO	2.46	2.49	2.38	2.49	2.60	3.02	2.90	3.17	3.20
MnO	0.35	0.32	0.31	0.36	0.29	0.13	0.15	0.06	0.11
TiO_2	0.05	0.04	0.54	0.02	0.10	0.04	0.03	0.04	0.03
Total	99.21	100.91	106.36	100.63	98.75	100.45	98.54	100.31	99.94
				Formula on the basis of 24 oxygen					
TSi	6.04	6.11	5.61	6.14	6.06	6.08	6.04	6.13	6.06
Fe+2	5.00	4.88	5.75	4.91	5.01	4.95	4.97	4.83	4.92
AlVI	4.14	4.19	3.44	4.13	4.11	4.13	4.17	4.17	4.14
Ca	0.18	0.18	0.16	0.17	0.13	0.09	0.09	0.09	0.09
Mg	0.60	0.59	0.55	0.60	0.64	0.72	0.71	0.76	0.77
Mn	0.05	0.04	0.04	0.05	0.04	0.02	0.02	0.01	0.01
TAl	0.00	0.00	0.39	0.00	0.00	0.00	0.00	0.00	0.00
Ti	0.01	0.01	0.06	0.00	0.01	0.01	0.00	0.01	0.00
				End-member compositions					
Alm	85.80	85.68	88.49	85.75	86.18	8.62	85.87	84.90	84.99
Grs	3.10	3.15	2.47	2.95	2.22	1.59	1.57	1.62	1.41
Prp	10.27	10.40	8.42	10.40	10.92	12.49	12.19	13.31	13.27
Sps	0.83	0.76	0.63	0.86	0.69	0.30	0.36	0.14	0.25
Uv	0.00	0.01	0.00	0.05	0.00	0.00	0.00	0.03	0.08

Appendix B

Appendix B. Garnet-biotite analyses employed in P-T calculations and corresponding calculated temperatures (T76: [52], HL77: [53], FS78: [54], HS82: [55], PL83: [56], Dasg91: [57], B92-HW, B92-GS: [58]).

Analyses Points	Garnet analyses				Biotite analyses				Mg/(Mg+Fe+2)		KD	Garnet end-members				Biotite	
	Fe^{+2}	Mn	Mg	Ca	Ti	Al^{VI}	Fe^{+2}	Mg	Garnet	Biotite		Alm	Sps	Prp	Grs	X(Ti)	$X(Al^{vi})$
p.1	4.75	0.29	0.49	0.36	0.13	1.31	2.56	2.44	0.09	0.49	9.18	0.81	0.05	0.08	0.06	0.02	0.20
p.2	4.75	0.28	0.46	0.37	0.16	1.25	2.37	2.45	0.09	0.51	10.58	0.81	0.05	0.08	0.06	0.03	0.20
p.3	4.72	0.27	0.47	0.40	0.16	1.21	2.50	2.42	0.09	0.49	9.78	0.81	0.05	0.08	0.07	0.03	0.19
p.4	4.65	0.29	0.49	0.36	0.14	1.46	2.36	2.31	0.09	0.49	9.35	0.80	0.05	0.08	0.06	0.02	0.23
p.5	4.72	0.28	0.48	0.34	0.17	1.19	2.49	2.45	0.09	0.50	9.67	0.81	0.05	0.08	0.06	0.03	0.19
p.6	4.78	0.23	0.51	0.35	0.17	1.15	2.54	2.48	0.10	0.49	9.19	0.81	0.04	0.09	0.06	0.03	0.18
p.7	4.82	0.15	0.51	0.32	0.18	1.11	2.51	2.53	0.09	0.50	9.61	0.83	0.03	0.09	0.06	0.03	0.18
p.8	4.89	0.14	0.50	0.33	0.14	1.18	2.47	2.52	0.09	0.50	9.92	0.83	0.02	0.09	0.06	0.02	0.19
p.9	4.94	0.09	0.54	0.30	0.16	1.15	2.50	2.51	0.10	0.50	9.18	0.84	0.01	0.09	0.05	0.02	0.18
p.10	5.02	0.05	0.60	0.25	0.21	1.17	2.40	2.53	0.11	0.51	8.89	0.85	0.01	0.10	0.04	0.03	0.19

Analyses Points	T76	HL77	FS78	HS82	PL83	Dasg91	B92-HW	B92-GS	Average Pressure (kbar)
p.1	476.3	476.2	435.9	458.4	498.0	391.6	503.7	510.0	3.9
p.2	450.8	452.4	404.7	427.4	477.8	368.4	484.5	493.7	4.1
p.3	467.6	466.8	423.1	448.0	490.0	388.0	495.9	502.5	4.4
p.4	473.0	473.0	431.7	454.6	495.4	372.5	501.6	508.6	3.9
p.5	466.0	466.9	423.7	445.0	490.2	385.8	496.2	504.2	3.8
p.6	483.6	479.6	439.5	461.4	500.9	402.9	507.3	516.9	5.1
p.7	474.0	471.3	428.7	448.9	493.8	394.5	504.2	518.3	4.9

Appendix B. Continued.

Analyses Points	**T76**	**HL77**	**FS78**	**HS82**	**PL83**	**Dasg91**	**B92-HW**	**B92-GS**	**Average Pressure (kbar)**
p.8	467.3	465.4	421.1	441.3	488.8	386.4	499.7	514.3	4.9
p.9	484.8	480.2	440.3	458.9	501.4	400.2	513.7	530.5	5.2
p.10	486.4	483.7	445.5	461.5	504.4	393.5	519.9	539.6	4.4
Minimum	450.8	452.4	404.7	427.4	477.8	368.4	484.5	493.7	3.8
Maximum	486.4	483.7	445.5	461.5	504.4	402.9	519.9	539.6	5.2
Mean	473.0	471.6	429.4	450.6	494.1	388.4	502.7	513.9	4.5
Std. Dev.	10.8	9.2	11.9	10.8	7.8	11.0	9.8	13.5	0.5